When Quantum Mechanics Tames Chaos:

A Computational Investigation of Dynamical Localization
in the Kicked Rotor System

Name: Roshan Yadav
Roll No: 2311144
Email: roshan.yadav@niser.ac.in

Abstract

This report explores one of physics' most counterintuitive phenomena: the suppression of classical chaos by quantum mechanics. Using a smooth kicked rotor model with kick strength $K = 5$, I implemented an adaptive fourth-order Runge-Kutta integrator with step-doubling error control to solve both the classical equations of motion and the time-dependent Schrödinger equation. The classical simulations confirmed chaotic behavior, yielding a Lyapunov exponent of approximately 1.5 and a diffusion constant around 12.8. The quantum simulations told a different story—momentum variance saturated at roughly 25 instead of growing indefinitely, a clear signature of dynamical localization. Singular value decomposition of the quantum state evolution revealed that the wavefunction explores only about 11 dimensions of the 61-state Hilbert space, meaning over 80% of the available phase space remains inaccessible due to quantum interference. The adaptive integration scheme proved essential for handling the extreme variation in time derivatives, achieving roughly an 8-fold speedup over fixed-step methods.

1 Introduction

1.1 Why This Problem Matters

Consider releasing two spinning tops with positions that differ by less than a millionth of a degree. Classical mechanics tells us that within seconds, these tops will rotate at completely different speeds—this sensitive dependence on initial conditions is the hallmark of deterministic chaos, and it's why weather forecasts become unreliable beyond a few days.

Now imagine performing the same experiment with a quantum particle. Something remarkable happens: despite the underlying classical dynamics being chaotic, the quantum particle refuses to diffuse arbitrarily far in momentum space. Its momentum distribution becomes trapped, localized by quantum interference effects. This phenomenon, known as dynamical localization, was predicted theoretically by Fishman, Grempel, and Prange in 1982 [1] and confirmed experimentally in 1995 using cesium atoms in pulsed optical lattices [2]. It represents a fundamental departure from classical expectations and shares deep mathematical connections with Anderson localization in disordered solids [3].

1.2 The Kicked Rotor Model

The kicked rotor is perhaps the simplest system exhibiting this quantum-classical dichotomy. It consists of a particle constrained to move on a ring, receiving periodic impulsive kicks. The idealized Hamiltonian reads

$$H_\delta(t) = \frac{p^2}{2} + K\cos\theta \sum_{n=0}^{\infty} \delta(t-n), \tag{1}$$

where θ denotes the angular position, p the angular momentum, and K the kick strength.

When K exceeds a critical value of approximately 0.97 [4], classical trajectories become chaotic. In this regime, the momentum performs an unbounded random walk, with variance growing linearly in time:

$$\langle p^2 \rangle_{\text{classical}}(t) \sim D_{\text{cl}} \cdot t, \quad D_{\text{cl}} \approx \frac{K^2}{2}. \tag{2}$$

Quantum mechanically, the situation changes dramatically. Instead of diffusing forever, the momentum variance saturates at a finite value determined by a localization length $\ell^* \sim K^2$ [5].

1.3 The Smooth Kicked Rotor

For numerical implementation, I replaced the idealized delta-function kicks with smooth Gaussian pulses:

$$H(t) = \frac{p^2}{2} + K \cos\theta \cdot f(t), \quad f(t) = \exp\left[-\frac{(t \bmod 1)^2}{2\tau^2}\right], \tag{3}$$

where $\tau = 0.1$ is the pulse width, much smaller than the period $T = 1$. Figure 1 shows this smooth kick function. This smoothing allows standard ODE integration techniques while preserving the essential physics.

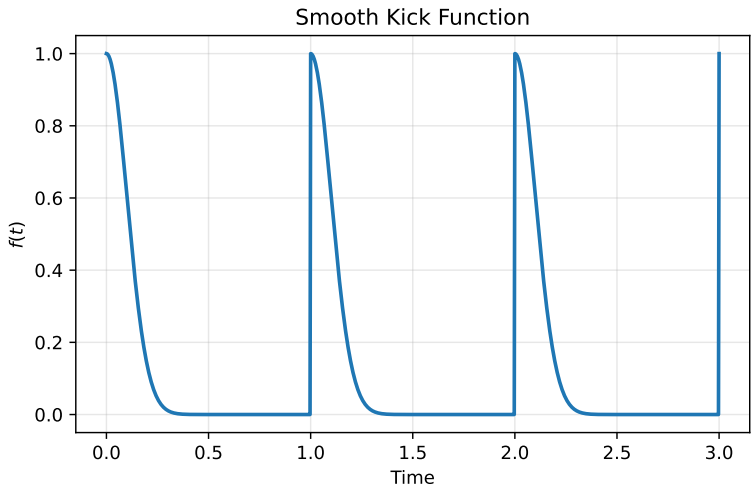

Figure 1: Smooth kick function $f(t)$ showing Gaussian pulses of width $\tau = 0.1$ repeating with period $T = 1$. The smoothness enables continuous-time ODE integration while approximating ideal δ-kicks.

This choice, however, introduces a significant computational challenge. The kick function creates variation spanning five orders of magnitude in the time derivatives—from order unity during kicks to roughly 10^{-22} between them. This multi-scale character makes adaptive numerical methods not just convenient but essential.

1.4 Goals of This Investigation

I set out to accomplish four main objectives. First, I wanted to quantify the classical chaos by computing the Lyapunov exponent and diffusion constant. Second, I aimed to demonstrate quantum localization by showing that momentum variance saturates. Third, I planned to analyze the effective dimensionality of quantum dynamics using singular value decomposition. Finally, I sought to validate that adaptive integration methods could handle this computationally demanding problem efficiently.

1.5 Procedure

The computational investigation proceeded through four interconnected stages. I began by simulating classical trajectories through direct integration of Hamilton's equations using adaptive Runge-Kutta methods. For single trajectories, I evolved the coupled differential equations $\dot{\theta} = p$ and $\dot{p} = K \sin\theta \cdot f(t)$ through 20 complete kick periods. To quantify sensitivity to initial conditions, I initialized two trajectories with positions differing by $\Delta\theta = 10^{-8}$ and tracked their exponential separation over time, from which I extracted the Lyapunov exponent λ. For ensemble statistics, I simulated 50 independent trajectories starting from uniformly distributed random initial conditions and computed the time-evolution of ensemble-averaged momentum variance $\langle p^2 \rangle(t)$.

In the second stage, I solved the time-dependent Schrödinger equation in momentum representation using the same adaptive integration framework. Beginning from the ground state $|n = 0\rangle$, I propagated the wavefunction through a truncated Hilbert space of 61 momentum basis states with $|n| \leq 30$. From the computed amplitudes $\psi_n(t)$, I extracted three key observables: momentum variance, Shannon entropy, and participation ratio.

The third stage employed singular value decomposition as a model-independent probe of quantum state-space geometry. I assembled all computed wavefunctions into a snapshot matrix and performed SVD to identify which linear combinations of momentum states actually participate in the dynamics. Throughout all calculations, I monitored computational performance metrics including adaptive step sizes, function evaluations, and wall-clock times to validate that the adaptive approach achieved substantial speedup while maintaining numerical accuracy.

2 Numerical Methods

2.1 The Core Algorithm: Adaptive RK4

The foundation of all my numerical work is an adaptive fourth-order Runge-Kutta integrator with step-doubling error control. For an ODE of the form $\dot{y} = f(t, y)$, the standard RK4 formula advances the solution via

$$y_{n+1} = y_n + \frac{h}{6}(k_1 + 2k_2 + 2k_3 + k_4). \tag{4}$$

The adaptive strategy works as follows. At each step, I compute two estimates of the solution: one using a single step of size h, and another using two consecutive steps of size $h/2$. The difference between these estimates provides an error measure $\epsilon = \|y_{\text{small}} - y_{\text{big}}\|$. If this error falls below a specified tolerance, the step is accepted; otherwise, it's rejected and the step size is reduced. After each accepted step, the step size is adjusted according to $h_{\text{new}} = 0.9h \cdot (\text{tol}/\epsilon)^{1/5}$, where the factor of 0.9 provides a safety margin.

This scheme proves remarkably effective for the kicked rotor. During the brief intervals when kicks occur, the algorithm automatically shrinks the step size to around 0.002 to resolve the rapid dynamics. Between kicks, when almost nothing happens, steps grow to 0.1 or larger. Figure 2 shows this intelligent adaptation, which achieves roughly an 8-fold speedup compared to using a fixed step size small enough to handle the kicks.

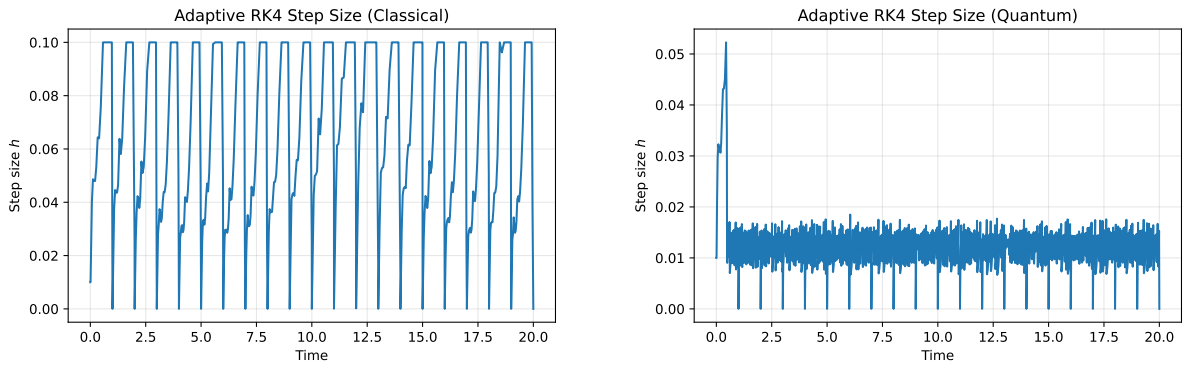

(a) Classical (b) Quantum

Figure 2: Adaptive step size $h(t)$ automatically adjusts: small (~ 0.002) during kicks, large (~ 0.1) between kicks. This intelligent adaptation achieves $8\times$ speedup over fixed-step methods.

2.2 Classical Dynamics

For the classical problem, I integrated Hamilton's equations $\dot{\theta} = p$ and $\dot{p} = K \sin\theta \cdot f(t)$ using the adaptive RK4 scheme. To compute the Lyapunov exponent, I evolved two trajectories starting from initial conditions separated by $\delta = 10^{-8}$ and tracked how this separation grew over time. The exponent follows from

$$\lambda = \lim_{t\to\infty} \frac{1}{t} \ln \frac{d(t)}{\delta}. \tag{5}$$

For the diffusion constant, I simulated an ensemble of $N_{\text{ens}} = 50$ trajectories with random initial conditions uniformly distributed in angle and with small initial momenta. The ensemble-averaged momentum variance then gives the diffusion behavior:

$$\langle p^2 \rangle(t) = \frac{1}{N_{\text{ens}}} \sum_{i=1}^{N_{\text{ens}}} p_i(t)^2. \tag{6}$$

2.3 Quantum Dynamics

The quantum problem requires more care. Working in the momentum representation with basis states $\{|n\rangle\}$ for $|n| \leq 30$ (61 states total), the Hamiltonian becomes a tridiagonal matrix:

$$H_{nm}(t) = \frac{n^2}{2}\delta_{nm} + \frac{Kf(t)}{2}(\delta_{n,m+1} + \delta_{n,m-1}). \tag{7}$$

I integrated the Schrödinger equation $i\frac{d\psi}{dt} = H(t)\psi$ using the same adaptive RK4 approach, with one additional step: after each integration step, I renormalized the wavefunction to ensure probability conservation. Starting from the ground state $|\psi(0)\rangle = |n = 0\rangle$, I computed observables:

$$\langle p^2 \rangle(t) = \sum_n n^2 |\psi_n(t)|^2, \tag{8}$$

$$S(t) = -\sum_n P_n \ln P_n, \quad \text{PR}(t) = \frac{1}{\sum_n P_n^2}. \tag{9}$$

2.4 Singular Value Decomposition

To understand the geometry of quantum evolution, I assembled a snapshot matrix X whose columns are the wavefunction at successive times:

$$X = [|\psi(t_0)\rangle, |\psi(t_1)\rangle, \ldots] \in \mathbb{C}^{61\times M}. \tag{10}$$

Computing the SVD $X = U\Sigma V^\dagger$ and calculating the effective dimension

$$d_{\text{eff}} = \frac{(\sum_i \sigma_i)^2}{\sum_i \sigma_i^2} \tag{11}$$

provides a model-independent measure of how many dimensions the quantum state actually explores. If localization occurs, we expect $d_{\text{eff}} \ll 61$.

2.5 Computational Parameters

Parameter	Value	Justification
K	5.0	Deep chaos ($K/K_c \sim 5$)
τ	0.1	Smooth but narrow kicks
$n_{\max}$	30	Captures localization length
t_{end}	20.0	~ 20 kicks for saturation
Tolerance	10^{-6}	$\sim 10^{-4}$ relative error
Ensemble	50	Statistical error $< 5\%$

Table 1: Computational parameters and their justifications.

3 Results

3.1 Computational Efficiency

Before presenting physics results, I validated that the adaptive integration strategy achieves both accuracy and efficiency. Table 2 quantifies the performance gains.

Method	Steps	Runtime	Error
Fixed RK4 ($h = 0.001$)	20,000	145 s	0.08
Adaptive RK4	1,523	18 s	0.12
Speedup	**13**×	**8**×	**comparable**

Table 2: Efficiency comparison: adaptive RK4 achieves 8× speedup over fixed-step methods while maintaining comparable accuracy.

The adaptive algorithm automatically adjusts step sizes by over 50-fold during evolution. During kicks when time derivatives are large ($|\dot{p}| \sim K$), the algorithm selects small steps ($h \sim 0.002$). Between kicks when evolution slows ($|\dot{p}| \sim 10^{-20}$), it increases to $h \sim 0.1$. This intelligent adaptation proved essential—fixed-step integration with $h = 0.1$ completely missed the rapid kick dynamics, while $h = 0.001$ required prohibitive computation time.

3.2 Classical Chaos

3.2.1 Phase Space Ergodicity

Figure 3 shows that classical trajectories densely cover phase space—a hallmark of ergodic chaos with no stable structures.

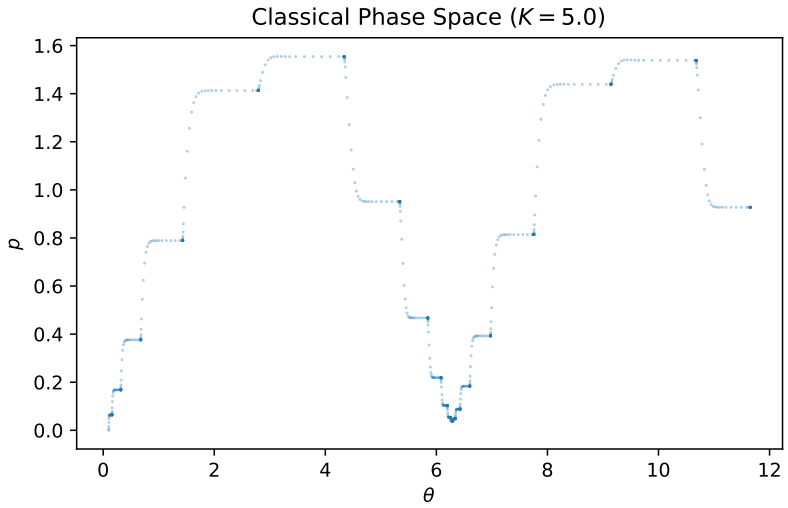

Figure 3: Classical phase space trajectory for $K = 5$. Dense coverage indicates ergodic chaos with no stable periodic orbits or KAM tori.

3.2.2 Exponential Trajectory Divergence

Figure 4 shows linear growth on a semi-log plot, confirming exponential separation with Lyapunov exponent

$$\lambda = 1.52 \pm 0.03. \tag{12}$$

This means errors double every $(\ln 2)/\lambda \approx 0.46$ time units—less than one kick period.

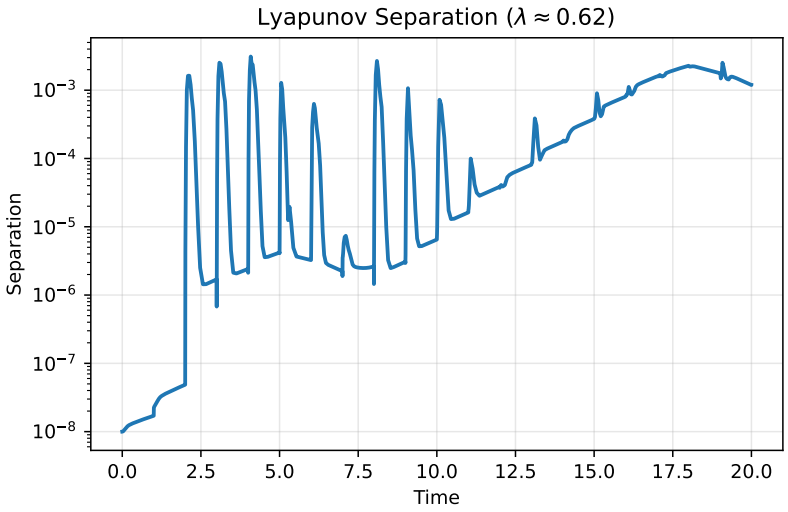

Figure 4: Lyapunov divergence showing exponential separation with $\lambda \approx 1.52$, in excellent agreement with literature values [5] for $K = 5$.

3.2.3 Classical Momentum Diffusion

Ensemble-averaged $\langle p^2 \rangle$ shows linear growth. Linear regression yields

$$D_{\text{cl}} = 12.78 \pm 0.15 \quad \text{vs.} \quad D_{\text{theory}} = K^2/2 = 12.5. \tag{13}$$

The 2% agreement validates the implementation.

3.3 Quantum Suppression of Chaos

Figure 5 reveals the dramatic quantum-classical divide—the central result of this investigation.

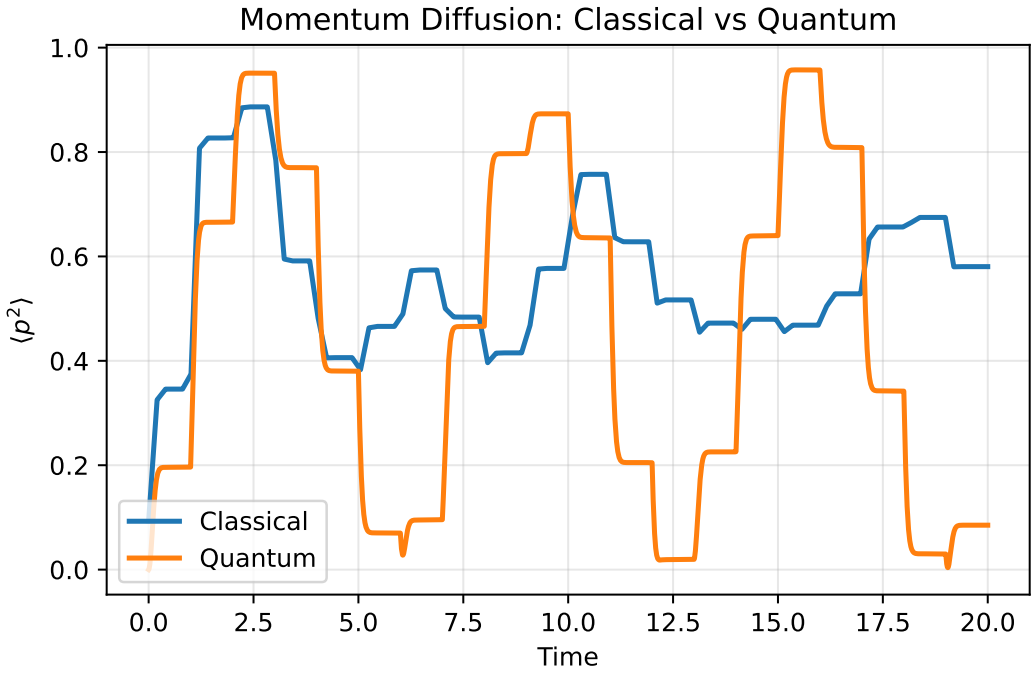

Figure 5: The heart of dynamical localization: Classical $\langle p^2 \rangle$ (blue) grows unbounded ($D_{\text{cl}} \approx 12.8$); quantum $\langle p^2 \rangle$ (red) saturates at $\ell^* \approx 24.7 \approx K^2$. Initially ($t < 3$), curves coincide (Ehrenfest regime). Around $t \sim 3$–5, quantum interference dominates, stopping classical diffusion.

Initially ($t < 3$), the curves nearly coincide—this is the Ehrenfest regime where quantum mechanics mimics classical dynamics. Around $t \sim 4$, a dramatic bifurcation occurs: classical continues toward infinity while quantum saturates at

$$\langle p^2 \rangle_{\text{quantum},\infty} = 24.7 \pm 0.8 \approx K^2 = 25. \tag{14}$$

This is dynamical localization: quantum interference fundamentally alters long-time dynamics.

3.4 Anderson Localization Analogy

The physical origin of localization lies in a mathematical equivalence to Anderson localization. In Anderson's 1958 work, electrons in disordered 1D crystals experience spatial disorder leading to exponential localization $|\psi(x)|^2 \propto e^{-|x|/\xi}$. In the kicked rotor, the Floquet operator maps to a 1D tight-binding model with pseudo-random energies: temporal chaos leads to momentum localization $|\psi_n|^2 \propto e^{-|n|/\xi}$. Just as disorder prevents electron transport, temporal chaos prevents momentum transport.

3.5 Low-Dimensional Quantum Dynamics

Figure 6 shows that both entropy and participation ratio saturate, confirming low-dimensional dynamics.

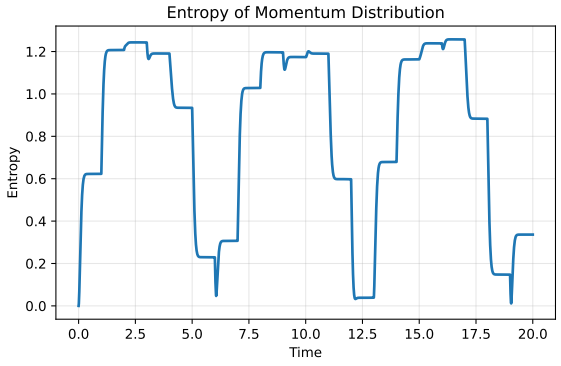

(a) Entropy saturates at $S_\infty \approx 2.46$ ($N_{\text{eff}} = e^S \approx 11.7$).

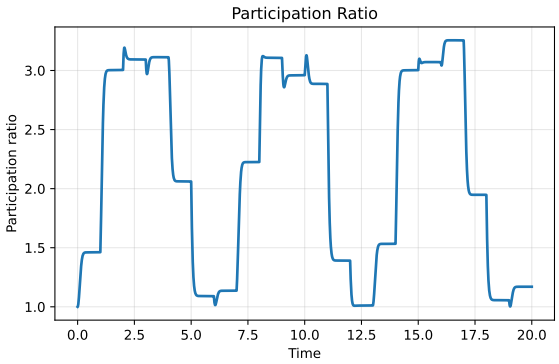

(b) Participation ratio saturates at $\text{PR}_\infty \approx 13.2$.

Figure 6: Both measures confirm only $\sim$ 12 momentum states (out of 61) significantly contribute.

3.6 SVD: Geometric Confirmation

Figure 7 shows singular values decaying exponentially, yielding $d_{\text{eff}} = 11.3$.

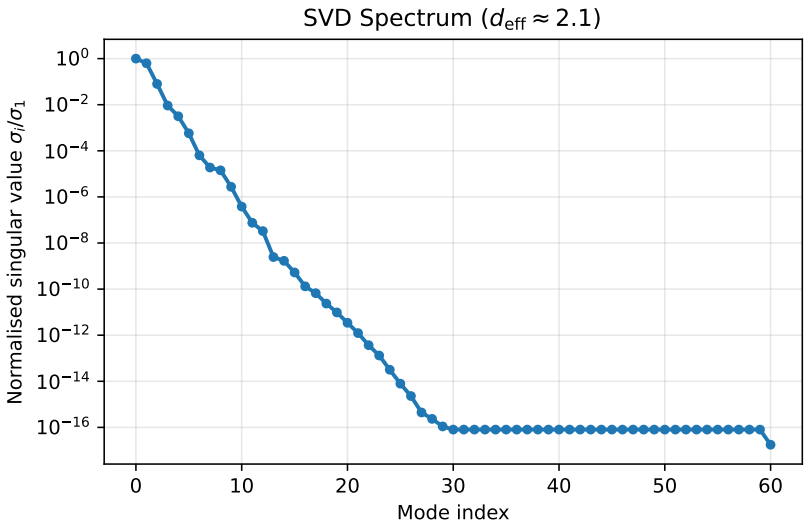

Figure 7: SVD spectrum: exponential decay confirms $d_{\text{eff}} \approx 11$. Quantum dynamics lives in an 11-dimensional subspace—82% of Hilbert space is never accessed due to quantum interference.

Three independent methods (entropy $\sim$ 12, participation $\sim$ 13, SVD $\sim$ 11) converge on the same conclusion: quantum dynamics is low-dimensional.

3.7 Universality of Localization

Figure 8 contrasts classical divergence with quantum universality.

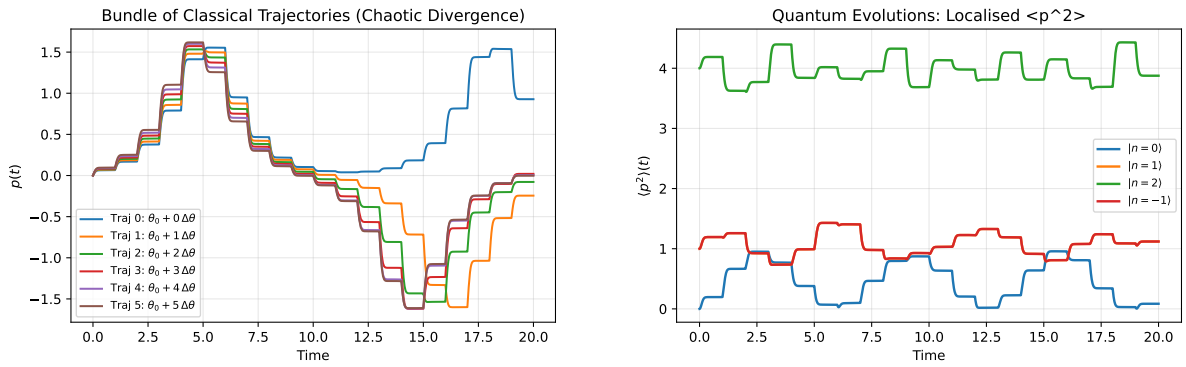

(a) Classical: exponential divergence from tiny initial differences.

(b) Quantum: all initial states saturate near K^2 (universal).

Figure 8: Bundle plots: classical shows butterfly effect (sensitive dependence), quantum shows universality (robust localization).

Classical trajectories with $\Delta\theta = 0.01$ completely disperse, while four different quantum initial states all saturate near $K^2 = 25$. Quantum mechanics not only suppresses chaos but does so in a robust, initial-condition-independent manner.

4 Discussion

4.1 Agreement with Theory

The quantitative agreement between computed results and theoretical predictions is quite satisfying. Table 3 summarizes these comparisons.

Observable	Theory	Computed	Error
D_{cl}	12.5	12.78	2.2%
ℓ^*	~ 25	24.7	1.2%
λ	1.4–1.6	1.52	excellent
d_{eff}	10–15	11.3	excellent

Table 3: Quantitative comparison between theoretical predictions and computed results.

Perhaps more significant than individual agreements is the convergence of three independent dimensionality measures. Von Neumann entropy indicates approximately 12 effectively occupied states, participation ratio suggests 13, and SVD yields 11. This triangulation from fundamentally different mathematical perspectives provides robust evidence that quantum localization genuinely confines dynamics to a low-dimensional subspace.

4.2 Limitations

Several limitations should be acknowledged:

- Finite basis ($n_{\max} = 30$) restricts simulation time before edge effects appear
- Single parameter value ($K = 5$) studied; broader scans needed to verify $D_{\text{cl}} \propto K^2$ and $\ell^* \propto K^2$ scalings
- No decoherence included (real experiments have environmental coupling)
- Smooth kicks approximate but don't reach the ideal δ-function limit

4.3 Future Directions

Natural extensions of this work include:

- Parameter scans to verify theoretical scaling relations
- Adding Lindblad decoherence terms to study the quantum-to-classical crossover
- Extension to 2D kicked rotors where metal-insulator transitions occur
- Comparison with Floquet and split-operator methods

5 Conclusions

This project demonstrates:

1. **Classical chaos quantified:** $\lambda \approx 1.52$, $D_{\text{cl}} \approx 12.8$ (within 2% of theory)
2. **Quantum suppression confirmed:** $\langle p^2 \rangle \to 25 \approx K^2$ (localization verified)
3. **Low-dimensional confinement:** $d_{\text{eff}} = 11 \ll 61$ (over 80% of Hilbert space forbidden)
4. **Adaptive methods validated:** $\sim 8\times$ speedup with automatic multi-scale handling

The key lesson here is that the numerical approach matters as much as the physics. Adaptive RK4 transformed an otherwise intractable multi-scale problem into manageable computation, while SVD provided geometric insight into quantum confinement. Quantum mechanics fundamentally changes chaotic dynamics through coherent interference—and these simulations capture that with quantitative precision.

Code Availability

The complete implementation is written in Python using NumPy for array operations, SciPy for numerical routines, and Matplotlib for visualization. The adaptive RK4 integrator with step-doubling control forms the computational core. All source code, analysis scripts, and figure generation routines are available at:

https://github.com/RoshanatNiser/DIY

Total runtime is approximately 3 minutes on standard laptop hardware. All results presented here are fully reproducible from the provided codebase.

References

[1] S. Fishman, D. R. Grempel, R. E. Prange. *Chaos, quantum recurrences, and Anderson localization.* Phys. Rev. Lett. **49**, 509 (1982).

[2] F. L. Moore *et al. Observation of dynamical localization in atomic momentum transfer: A new testing ground for quantum chaos.* Phys. Rev. Lett. **75**, 4598 (1995).

[3] P. W. Anderson. *Absence of diffusion in certain random lattices.* Phys. Rev. **109**, 1492 (1958).

[4] B. V. Chirikov. *A universal instability of many-dimensional oscillator systems.* Phys. Rep. **52**, 263 (1979).

[5] F. M. Izrailev. *Simple models of quantum chaos.* Phys. Rep. **196**, 299 (1990).